Human Microtubule-Associated-Protein Tau Regulates the Number of Protofilaments in Microtubules: A Synchrotron X-Ray Scattering Study

M. C. Choi,[†‡§‖*] U. Raviv,[†‡§] H. P. Miller,[§] M. R. Gaylord,[§¶] E. Kiris,[§¶] D. Ventimiglia,[§¶] D. J. Needleman,[†‡§] M. W. Kim,[‖*] L. Wilson,[§¶] S. C. Feinstein,[§¶*] and C. R. Safinya[†‡§*]

[†]Materials, [‡]Physics, [§]Molecular, Cellular, and Developmental Biology Departments, and [¶]Neuroscience Research Institute, University of California, Santa Barbara, California 93106; and [‖]Department of Physics, KAIST, Daejeon 305-701, Korea

ABSTRACT Microtubules (MTs), a major component of the eukaryotic cytoskeleton, are 25 nm protein nanotubes with walls comprised of assembled protofilaments built from $\alpha\beta$ heterodimeric tubulin. In neural cells, different isoforms of the microtubule-associated-protein (MAP) tau regulate tubulin assembly and MT stability. Using synchrotron small angle x-ray scattering (SAXS), we have examined the effects of all six naturally occurring central nervous system tau isoforms on the assembly structure of taxol-stabilized MTs. Most notably, we found that tau regulates the distribution of protofilament numbers in MTs as reflected in the observed increase in the average radius $\langle R^{MT} \rangle$ of MTs with increasing Φ, the tau/tubulin-dimer molar ratio. Within experimental scatter, the change in $\langle R^{MT} \rangle$ seems to be isoform independent. Significantly, $\langle R^{MT} \rangle$ was observed to rapidly increase for $0 < \Phi < 0.2$ and saturate for Φ between 0.2–0.5. Thus, a local shape distortion of the tubulin dimer on tau binding, at coverages much less than a monolayer, is spread collectively over many dimers on the scale of protofilaments. This implies that tau regulates the shape of protofilaments and thus the spontaneous curvature C_o^{MT} of MTs leading to changes in the curvature C^{MT} ($=1/R^{MT}$). An important biological implication of these findings is a possible allosteric role for tau where the tau-induced shape changes of the MT surface may effect the MT binding activity of other MAPs present in neurons. Furthermore, the results, which provide insight into the regulation of the elastic properties of MTs by tau, may also impact biomaterials applications requiring radial size-controlled nanotubes.

INTRODUCTION

Microtubules (MTs) are among the major filamentous elements of the eukaryotic cytoskeleton involved in a range of cellular functions including intracellular trafficking, cell division, and the establishment and maintenance of cell shape (1). They consist of hollow 25 nm diameter protein nanotubes, comprised of globular dimeric $\alpha\beta$ tubulin subunits (with a net charge of $-41e$) aligned end-to-end to form linear protofilaments, which interact laterally to form the hollow MT cylinder (Fig. 1 *A*). The number of protofilaments (N_{pf}) per MT averages 13, however, MTs have been reported with as few as 11 or as many as 15 (2–5). Although MTs exhibit dynamic instability (cycles of rapid shortening followed by slow growth) in dividing cells, they tend to be less dynamic in the axons and dendrites of neuronal cells. A variety of different microtubule-associated-proteins (MAPs) regulate MT dynamics, although their precise mechanisms of action are not well understood (6). Previous work has shown that the neural MAP tau enhances tubulin assembly both in vivo (7–9) and in vitro (10,11), and that it is required for the establishment of neuronal cell polarity (12), and the outgrowth and maintenance of neuronal axons (9,13). Further, aberrant tau action has long been correlated with numerous neurodegenerative diseases, including Alzheimer's, Pick's, supranuclear palsy, and fronto-temporal dementia with Parkinsonism linked to chromosome 17 (FTDP-17) (14,15). More recent genetic analyses have demonstrated unequivocally that errors in tau action and/or regulation cause neuronal cell death and dementia in many of these disorders (16–18).

In the mammalian adult central nervous system (CNS), alternative RNA splicing generates six different tau isoforms (19), which are widely believed to be unstructured in solution (20). The overall positively charged MT binding regions of tau isoforms contain either three or four imperfect repeats (18 amino acids in length and designated as 3R-tau or 4R-tau, respectively), separated from one another by interrepeat segments (13–14 amino acids in length), resulting from exclusion or inclusion of exon 10 encoded sequences (Fig. 1 *B*) (21–24). The repeat region is flanked by a proline-rich basic region and the C-terminal tail. Upstream of the proline-rich region is the N-terminal tail, which can contain either zero, one, or two 29 amino acid long inserts resulting from the exclusion or inclusion of exon 2 and/or 3 encoded sequences, thereby giving rise to short (S-), medium (M-), and long (L-) N-terminal projection domains (Fig. 1 *B*). Expression of the six different tau isoforms is developmentally regulated. More specifically, whereas fetal brain expresses only the shortest isoform (3RS), adult human brain expresses an ~1:1 ratio of 3R and 4R tau, in all combinations with the three different (S-, M-, L-) N-terminal region configurations (25). Further, genetic mutations that alter

Submitted December 29, 2008, and accepted for publication April 28, 2009.

*Correspondence: safinya@mrl.ucsb.edu, feinstei@lifesci.ucsb.edu, mcchoi@mrl.ucsb.edu, or mwkim@kaist.ac.kr

U. Raviv's present address is The Chemistry Institute, Hebrew University of Jerusalem, Givat Ram 91904, Israel.

D. J. Needleman's present address is School of Engineering and Applied Science; Molecular and Cellular Biology and FAS Center for Systems Biology, Harvard University, Cambridge, MA 02138.

Editor: Marileen Dogterom.

0006-3495/09/07/0519/9 $2.00

doi: 10.1016/j.bpj.2009.04.047

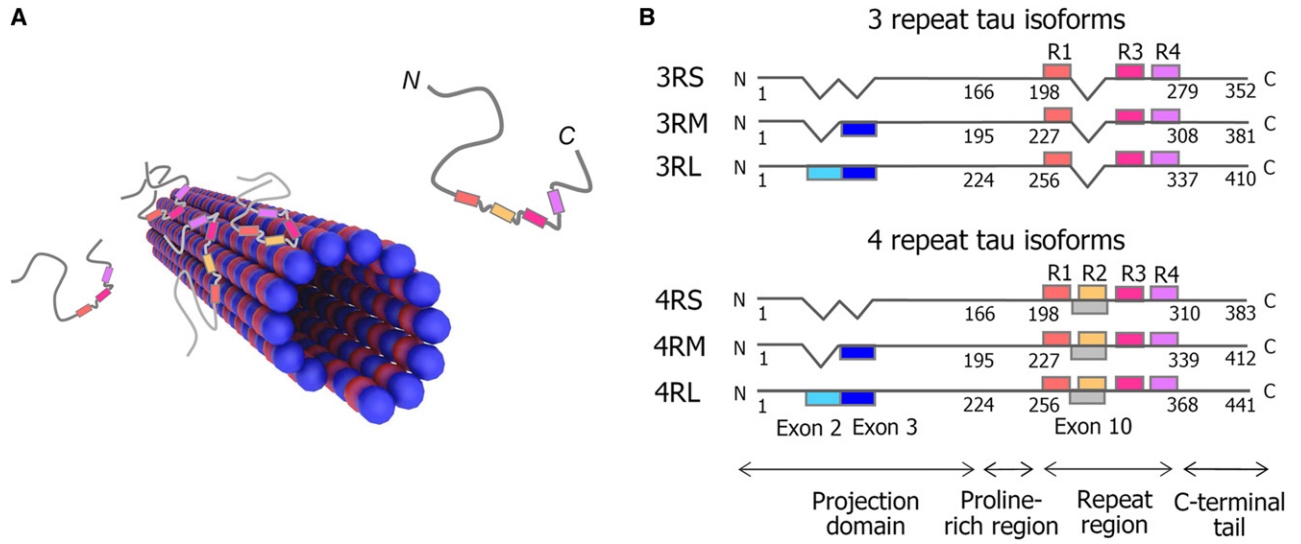

FIGURE 1 (*A*) Schematic of a MT decorated with adsorbed tau isoforms. (*B*) Six isoforms of human wild-type tau. tau isoforms possess either three or four imperfect repeats (R), which differ by exclusion or inclusion of a 31 amino acids that contain R2 and interrepeat between R1 and R2. Isoforms also differ in the N-terminal region by possessing either zero, one, or two 29 amino acids, thereby generating short (S-), medium (M-), or long (L-) isoforms. The numbers below each isoform refer to the first residue of the isoform, the beginning residues for the proline-rich region, the repeat region, and the C-terminal tail, and the last residue of the isoform.

the normal 1:1 ratio of 3R to 4R tau lead to neuronal cell death and dementia in FTDP-17 and related tauopathies, showing clearly that there must be some functional and/or regulatory differences between 3R and 4R tau isoforms (16–18).

We have used synchrotron small angle x-ray scattering (SAXS) and biochemical binding assays to probe changes in the structure of taxol-stabilized MTs on binding by the six different human CNS tau isoforms. SAXS showed that the average MT radius $\langle R^{\mathrm{MT}} \rangle$ increased as a function of increasing density of tau isoforms bound to MTs indicating that addition of tau increases $\langle N_{\mathrm{pf}} \rangle$ by regulating the distribution of protofilament numbers in MTs. Within the context of an elastic description of a MT our finding implies that tau regulates the spontaneous curvature of MTs. Interestingly, within experimental scatter, all six isoforms seem to qualitatively exhibit the same effect. Further, we find that tau-MT interactions are mediated to a large extent via nonspecific electrostatic interactions: tau binding affinity decreases with increasing KCl concentration, resulting in desorption of tau molecules from MT surfaces and a decrease in $\langle R^{\mathrm{MT}} \rangle$.

MATERIALS AND METHODS

Purification of tau and tubulin/Microtubule assembly/Tau-microtubule mixtures

Tau was expressed and purified as described (26). Briefly, tau was expressed in BL21 (DE3) cells (Novagen, Madison, WI). Bacteria were lysed by sonication and boiled for 10 min. Heat-stable proteins were isolated by centrifugation, bound to a phosphocellulose column and eluted with a salt gradient (0.2–1.0 M NaCl). tau-containing fractions were pooled and further purified using reverse-phase HPLC (DeltaPak-C18; Millipore, Billerica, MA). HPLC fractions containing tau were pooled, lyophilized, and resuspended in BRB_{80} buffer (80 mM Pipes pH 6.8, 1 mM EGTA, 1 mM MgSO_4) with 0.1% β-mercaptoethanol. The concentration of each tau sample was determined by SDS-PAGE comparison with a tau mass standard, the concentration of which was established by amino acid analysis (27).

Tubulin was purified, as described (28). Briefly, MAP-rich bovine brain MT protein was prepared by two cycles of assembly and disassembly. Tubulin was purified from other MT proteins by elution through a Whatman P-11 phosphocellulose column equilibrated in PEM_{50} (50 mM Pipes, 1 mM MgCl_2, 1 mM EGTA, 0.1 mM GTP). Purified tubulin (>99% pure) was drop frozen in liquid nitrogen and stored at −70°C. MTs were assembled at 35°C for 20 min from 45 μM (5 mg/mL) tubulin in PEM_{50} buffer (50 mM Pipes, 1 mM EGTA, 1 mM MgCl_2, pH 6.8) in the presence of 1 mM GTP and 5 wt % glycerol (with a final tubulin concentration of 40 μM (4.4 mg/mL)), and then stabilized by 40 μM taxol (2 mM taxol in DMSO was added in a stepwise manner). tau was added to preassembled MTs at the desired tau/tubulin-dimer molar ratio. The tau-MT samples used in all experiments were prepared such that they were in buffer comprised of nearly equal volumes of PEM_{50} and BRB_{80}. A small volume of a 1 M KCl in PEM_{50}/BRB_{80} buffer was added to each tau-MT mixture to achieve the desired salt concentration. The samples in Figs. 2–5 were prepared with a final concentration of 25 mM of KCl.

Microtubule/tau binding assay

Taxol stabilized MTs (prepared from 15 μM tubulin) were mixed at varying molar ratios of tau to tubulin-dimer ($\Phi = N_{\mathrm{tau}}/N_{\mathrm{tubulin\text{-}dimer}}$) layered over an 80 μL sucrose cushion (50% sucrose in $\mathrm{PEM}_{50}/\mathrm{BRB}_{80}$) in 5 × 20 mm ultraclear centrifuge tubes (Beckman Instruments, Palo Alto, CA) and centrifuged in an Airfuge (Beckman Instruments) for 12 min at 150,000 × g at room temperature. Supernatants and pellets were harvested and solubilized in SDS-PAGE sample buffer. Relative amounts of tau in the supernatants and pellets were determined by SDS-PAGE and immunoblotting with the monoclonal antibody tau-1 and tubulin in the supernatants and pellets by SDS-PAGE and dye bound intensity analysis (29,30).

Synchrotron SAXS

SAXS was carried out at the Stanford Synchrotron Radiation Laboratory beam-line BL 4-2 at 9 keV. A 2D area detector MarCCD (MarUSA, Evanston,

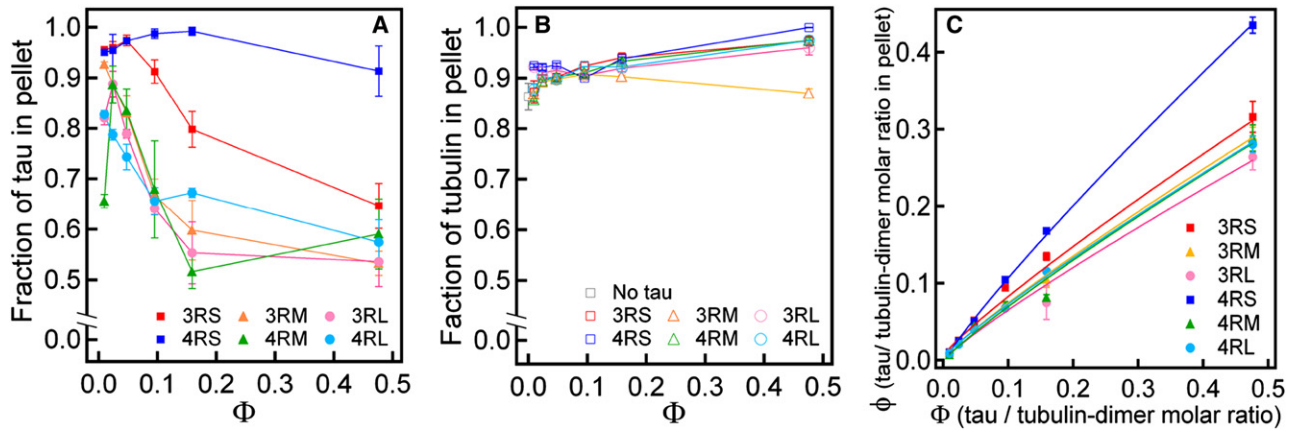

FIGURE 2 Assays measuring the distinct binding of tau isoforms to the MT surface. Fraction of tau (*A*) and tubulin (*B*) in pellets as a function of the tau/tubulin-dimer molar ratio in the reaction mixture (Φ) for each of the six tau isoforms. (*C*) Plot of ϕ (tau/tubulin-dimer in pellets) versus Φ. ϕ measures the fraction of tau bound to the MT surface whereas Φ takes into account all tau (attached and in buffer) and all tubulin (in MTs and in buffer).

IL) was used to collect the powder scattering patterns. Sample to detector distance was set to be 2.5 m and silver behenate was used as a standard to calibrate the momentum transfer q. The images were azimuthally integrated to give scattering intensity versus momentum transfer q. Samples were spun down at 16,000 × g for 30 min and loaded in 1.5 mm quartz capillaries.

Differential interference contrast and polarized light microscopy

Differential interference contrast (DIC) was measured using high sensitive CCD camera (SensiCam^{QE}, Cooke) mounted on an inverted microscope Diaphot 300 (Nikon) with Xenon lamp (Sutter Instrument, Novato, CA). An Optiphot 2-pol (Nikon, Melville, NY) was used for polarized microscopy.

Transmission electron microscopy

A JEM 1230 (JEOL) electron microscope was used with the electron beam set at 80 kV. MTs (0.1 mg/mL) were loaded on Formvar coated copper grid (Ted Pella, Redding, CA), and stained with 1 wt % uranyl acetate (Electron Microscopy Sciences, Hatfield, PA) in deionized water.

RESULTS AND DISCUSSION

Binding density of tau isoforms on microtubule surfaces

In Fig. 2, *A* and *B*, we show the results of assays measuring the distinct binding density of the six human tau isoforms to 40 μM taxol-stabilized microtubules. The figures plot the fractions of tau (Fig. 2 *A*) and tubulin-dimer (Fig. 2 *B*) present in pellets as a function of $\Phi = N_{tau}/N_{tubulin\text{-}dimer}$, the molar ratio of total tau to total tubulin-dimer in the original reaction mixtures (that includes tau adsorbed on MTs and in buffer, and tubulin in MTs and in buffer). Fig. 2 *B* shows that increasing the value of Φ promotes the assembly of the small pools of soluble tubulin left unassembled by taxol, with the possible exception of 3RM.

Fig. 2 *C*, which combines Fig. 2, *A* and *B*, plots the tau/tubulin molar ratio in the pellet ($\phi = \Phi \times f_{tau}/f_{tubulin\text{-}dimer}$) versus Φ. Here, f_{tau} and $f_{tubulin\text{-}dimer}$ are the fractions of tau and tubulin-dimer in the pellet, respectively. Thus, for each sample prepared at a given Φ, ϕ is a measure of the actual amount of tau bound to the MT surface, and is proportional to the tau binding density (number of tau molecules adsorbed to the MT surface per unit area). We observe that the ϕ increases as Φ increases and this is isoform-dependent, with 4RS tau packing much tighter on microtubules than any of the other isoforms, followed by 3RS tau. It is notable that the two tau isoforms that pack most tightly on taxol-stabilized microtubules are the ones with the smallest projection domains, lacking both N-terminal inserts. Although the N-terminal inserts do not bind directly to microtubules (21,23,31), these data suggest that they do confer an effect on the ability of tau to pack tightly on microtubules. At low coverage ($\Phi \approx 0.1$) where the tau isoforms are far from each other, the smaller binding affinity of isoforms with M- and L-projection domains is most likely due to the electrostatic repulsion between the negatively charged inserts and the MT surface (that is also overall negatively charged). At higher coverages (Φ between 0.15–0.5) with tau isoforms in close proximity, the effect could be primarily mediated by increased tau-tau electrostatic repulsion of the negatively charged inserts in neighboring medium and long tau isoforms.

Tau regulates the radial size distribution of microtubules

The microscopy and x-ray scattering data show unambiguously that none of the six tau isoforms induce bundles in 40 μM taxol-stabilized MTs for the range of tau concentrations explored in this study with $0 \leq \Phi \leq 1/2$. Fig. 3, *A* and *B*, show 1.5 mm quartz capillaries, filled with either MT (Fig. 3 *A*) or MT mixed with 3RS tau at $\Phi = 1/10$ (Fig. 3 *B*), viewed between crossed polarizers, with optical microscopy. The thread-like texture observed is due to a nematic liquid crystal phase of MTs; that is, where large domains of MTs are orientationally ordered but positionally

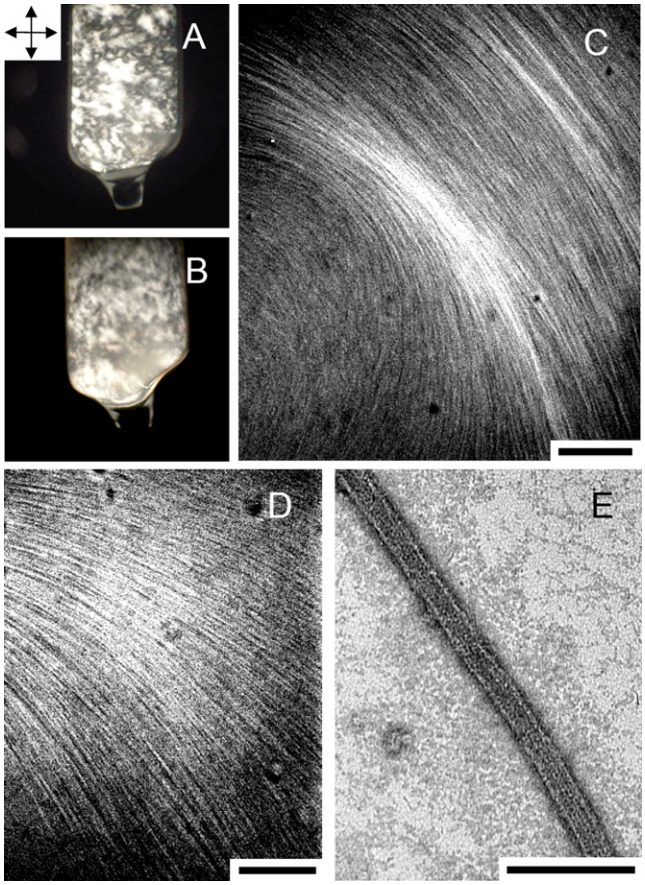

FIGURE 3 Light and transmission electron microscopy images of MTs with or without bound tau. Polarized light microscopy images of MTs (*A*) and 3RS tau-MTs at tau to tubulin-dimer molar ratio $\Phi = 1/10$ (*B*) in 1.5 mm quartz capillaries show thread-like nematic liquid crystalline texture. Differential interference contrast microscopy images show oriented and uniformly distributed MTs (*C*) and MTs with bound 3RS tau isoforms at $\Phi = 1/10$ (*D*) (scale bar, 10 μm). (*E*) TEM image of an MT with bound 3RS at $\Phi = 1/6$ (scale bar = 100 nm). MT concentrations were as follows: *A* and *C*, 4.4 mg/mL; *B*, 3.8 mg/mL; *D*, 2.2 mg/mL; and *E*, 0.1 mg/mL.

disordered as in a liquid. At higher magnification, DIC shows the presence of large oriented MT domains. Fig. 3 *C* is MTs in buffer, and Fig. 3 *D* is MTs mixed with 3RS tau at $\Phi = 1/10$. It is clear from the DIC images that the MTs are distributed uniformly . In contrast DIC of MT bundles are highly nonuniform indicative of local regions with a high density of MTs (32). Consistent with the optical microscopy, TEM also shows no evidence for MT bundles for $\Phi \leq 1/2$, but rather only individual MTs are observed. Fig. 3 *E* shows a typical example of an MT bound 3RS tau at $\Phi = 1/6$.

We used synchrotron SAXS experiments to examine the effect of tau binding on the structure of MTs on the Å-scale. Fig. 4 *A* shows SAXS profiles of 4RS tau mixed with taxol-stabilized MTs for $0 \leq \Phi \leq 1/2$. The shape of the scattering data is due entirely to the form factor F_{MT} of noninteracting MTs, in agreement with the DIC, polarized microscopy, and TEM observations (Fig. 3) for $\Phi \leq 1/2$, where no evidence of tau-induced bundling is observed. Consistent with previous work (32–34) we modeled MTs by assuming a hollow cylinder (i.e., a one-box model shown in Fig. 4 *B*, *inset*) and values for the wall thickness (49 Å) and radial electron density relative to water $\Delta\rho_{\mathrm{tubulin}} = 0.07817$ e/Å^3 that are consistent with published literature data (35–37). Thus, the SAXS intensity from the sample, consisting of randomly oriented domains, is $\propto |F_{\mathrm{MT}}|^2$ powder averaged over the wave-vector $\mathbf{q}$, where F_{MT} = Fourier transform of the MT electron density. The main parameter resulting from the fit of the SAXS data to this simple model is the average MT inner radius $\langle R_{\mathrm{in}}^{\mathrm{MT}} \rangle$. Furthermore, we also followed previous MT related x-ray structure work in subtracting a background that is comprised of a polynomial that passes through the scattering minima of the SAXS data (32–34).

The solid lines through the SAXS data of Fig. 4 *B* are the result of quantitative nonlinear least-squares fits of the model to the background subtracted data. For the data with no added tau the fit yielded $\langle R_{\mathrm{in}}^{\mathrm{MT}} \rangle = 77.9$ Å in good agreement with MTs comprised on average of 13 protofilaments (2–4,33,34). With increasing Φ (4RS-tau/tubulin-dimer) the SAXS profiles (Fig. 4, *A* and *B*) are seen to shift to lower q indicating an increase in $\langle R_{\mathrm{in}}^{\mathrm{MT}} \rangle$ or equivalently the mean protofilament number $\langle N_{\mathrm{pf}} \rangle$. Similar behavior is found for the other five isoforms of tau (see Fig. S1 in the Supporting Material). It is evident from the high quality of the fits that the model of a hollow cylinder at constant MT wall thickness and $\Delta\rho_{\mathrm{tubulin}}$, with $\langle R_{\mathrm{in}}^{\mathrm{MT}} \rangle$ as the sole parameter allowed to vary, gives a quantitative fit even for SAXS profiles of MT decorated with tau isoforms (Fig. 1 *A*). As we describe below, the reason that this simple one-box model is able to fit the data even with tau bound to the MT surface is because, for the tau coverages studied, the electron density contrast between the region containing tau relative to water is small.

As an alternative model we considered the possibility that the shift in the SAXS profile to lower q with increasing Φ resulted from the addition of tau on the outer MT surface, which tends to thicken the wall, at a constant protofilament number with a fixed microtubule inner radius of 77.9Å. In this alternative model the electron density profile consists of three boxes shown in Fig. 4 *C*: a tubulin wall region, a second region containing the bound portion of tau (4RS-tau residues 166–309 bound to tubulin dimers with thickness $\approx$ 10.88 Å consisting of an adsorbed hydrated unstructured polypeptide monolayer), and a third projection domain (4RS-tau residues 1–165) with a radius of gyration $R_{\mathrm{g}} = aN^{0.6} = 41.2$ Å, where $N = 165$ and the prefactor a was taken to be 1.927 Å consistent with published data for unstructured proteins (38). The result of the three-box model calculation for $\Phi_{4\mathrm{RS}}$ (4RS-tau/tubulin-dimer) = 1/10 is shown as solid line in Fig. 4 *D*, which systematically deviate from the measured SAXS profile and rule out this alternative model, which assumes a constant protofilament number $\langle N_{\mathrm{pf}} \rangle$.

The results of the fit of the simple one-box model to the data showing an increase in $\langle R_{\mathrm{in}}^{\mathrm{MT}} \rangle$ plotted versus Φ with

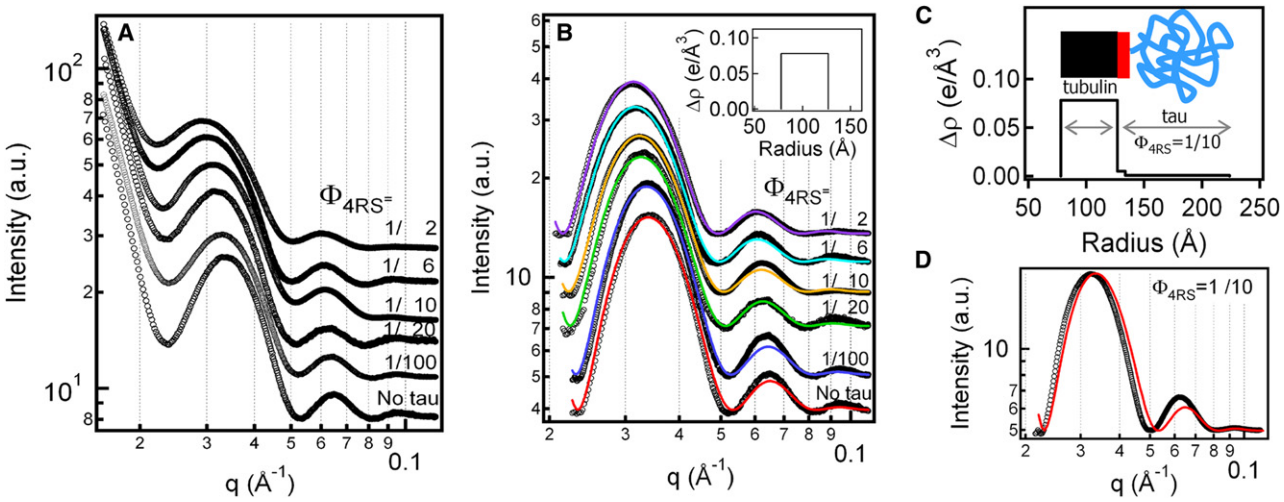

FIGURE 4 (*A* and *B*) SAXS data showing that tau regulates the mean radius of MTs, or equivalently, the MT protofilament number (N_{pf}). SAXS results of MTs with bound 4RS tau as a function of tau to tubulin-dimer molar ratio in the reaction mixture (Φ) before (*A*) and after (*B*) background subtraction. With increasing tau, the SAXS profile shifts to lower q implying an increase in the MT radius. Colored lines are results of fits of the data to the one-box model with the MT electron density shown in *B* (*inset*) (see Fig. S1 for SAXS results of five other tau isoforms). (*C*) The three-box electron density model description of MAP tau bound to the surface of a MT for Φ_{4RS} (4RS-tau/tubulin-dimer) = 1/10. The first box corresponds to the tubulin wall of the MT with an electron density relative to water = 0.07817 e/Å^3 (35–37) and thickness 49 Å. The second box is the region containing bound MAP tau, which consists of 144 residues comprising the repeat domains and the proline region (Fig. 1 *B*). The thickness is taken to be the diameter of an adsorbed hydrated unstructured polypeptide ≈ 10.88 Å; diameter = 6.88 Å plus a 2 Å hydration layer. (The diameter of polypeptide tau was estimated from the volume of tau (= weight of tau/mass density of tau (=1.41 g/cc)) and using a contour length of 3.5 Å × 383 residues.) The third box contains the N-terminus projection domain (165 residues) and the thickness of this region is assumed to be $2R_g$, where $R_g = 1.927N^{0.6} = 41.2$ Å (38). The electron densities (relative to water) for the second and third boxes (with bound and projection regions of tau) were taken to be 0.005 e/Å^3 and 0.0009 e/Å^3, respectively. They were calculated by estimating the fraction of tau in each region and using ρ (electron density) = tau-volume-fraction × ρ_{tau} + water-volume-fraction × ρ_{water}. The electron density of tau (ρ_{tau}) was taken to be 0.462 e/Å^3. The tau-volume-fractions were first calculated for tau/tubulin dimer = 1 (where each tubulin dimer is assumed to have one tau attached to its surface area 50 Å × 80 Å) and multiplied by ϕ (the actual tau/tubulin-dimer ratio). (*D*) The solid line, which does not fit the data, is the result of a calculation using the three-box model at a constant $\langle R_{in}^{MT}\rangle = 77.9$ Å (or equivalently protofilament number $\langle N_{pf}\rangle = 13$) described in *C* for Φ_{4RS} (4RS-tau/tubulin-dimer) = 1/10.

increasing tau for all six isoforms is shown in Fig. 5, *B–D*. The same data plotted versus ϕ, which only considers the fraction of tau bound to MTs, is shown in Fig. 5, *E–G*. The data show that $\langle R_{in}^{MT}\rangle$ increases from 77.9 Å (MT without tau) and saturate around 86.6 Å with added tau. This corresponds to an increase in the radius of MTs by ~8.7 Å, or ≈11.2%. This increase implies a shift in the mean number of protofilaments $\langle N_{pf}\rangle$ in MTs, shown schematically in Fig. 5 *A*, from 13 to 14 (see *y* axis label of Fig. 5, *B–G*) in terms of the mean protofilament number $\langle N_{pf}\rangle$). By comparing the data for all six isoforms one can see that the increase in the radial size due to added tau is isoform independent. We note, however, the there is a relatively large scatter in the data, which precludes the observation of small differences between different isoforms. The scatter in the data likely results both from small variations between independent protein preparations and the error in $\langle R_{in}^{MT}\rangle$ resulting from the fit of the data to the one-model (Fig. 4 *B*, *inset*).

We point out that the lack of information on the precise MAP-tau monomer concentration profile in the binding and projection domain regions prevents a more comprehensive line-shape analysis of the SAXS data beyond the one-box model used in this study. Nevertheless, the simple one-box model used in this study should be regarded as sufficient because, as seen in Fig. 5, most of the increase in $\langle R_{in}^{MT}\rangle$ occurs for Φ (4RS-tau/tubulin-dimer) $\leq$ 0.1, which amounts to a very small change in the electron density relative to water in the immediate region near the MT surface.

Noninteger values of $\langle N_{pf}\rangle$ measured in the SAXS data imply a variation in the distribution of protofilament numbers in MTs. For example, $\langle N_{pf}\rangle$ = 13.5 implies there are equal numbers of MTs with either 13 or 14 protofilaments (Fig. 5 *A*). As we described earlier the binding assay data show that taxol-stabilized MTs coexist with soluble tubulin for $0 \leq \Phi \leq 1/2$ (Fig. 2 *B*). Two previous AFM studies have also found that individual protofilaments coexist with taxol-stabilized microtubules (39,40). Thus, changes in $\langle N_{pf}\rangle$ may occur either due to exchanges of protofilaments between solvent and MTs or between neighboring MTs leading to a redistribution of protofilament numbers. Redistribution of protofilament number for MTs in vitro is known to occur under other conditions. In recent work it was found that cationic lipid bilayers coating taxol-stabilized MTs also induce changes in $\langle N_{pf}\rangle$ that are dependent on the charge density of the lipid bilayer (33). Our recent SAXS data also show that the average MT radius decreases as the taxol concentration increases between 10 μM and 40 μM (M. C. Choi, S. C. Feinstein, and C. R. Safinya, unpublished data).

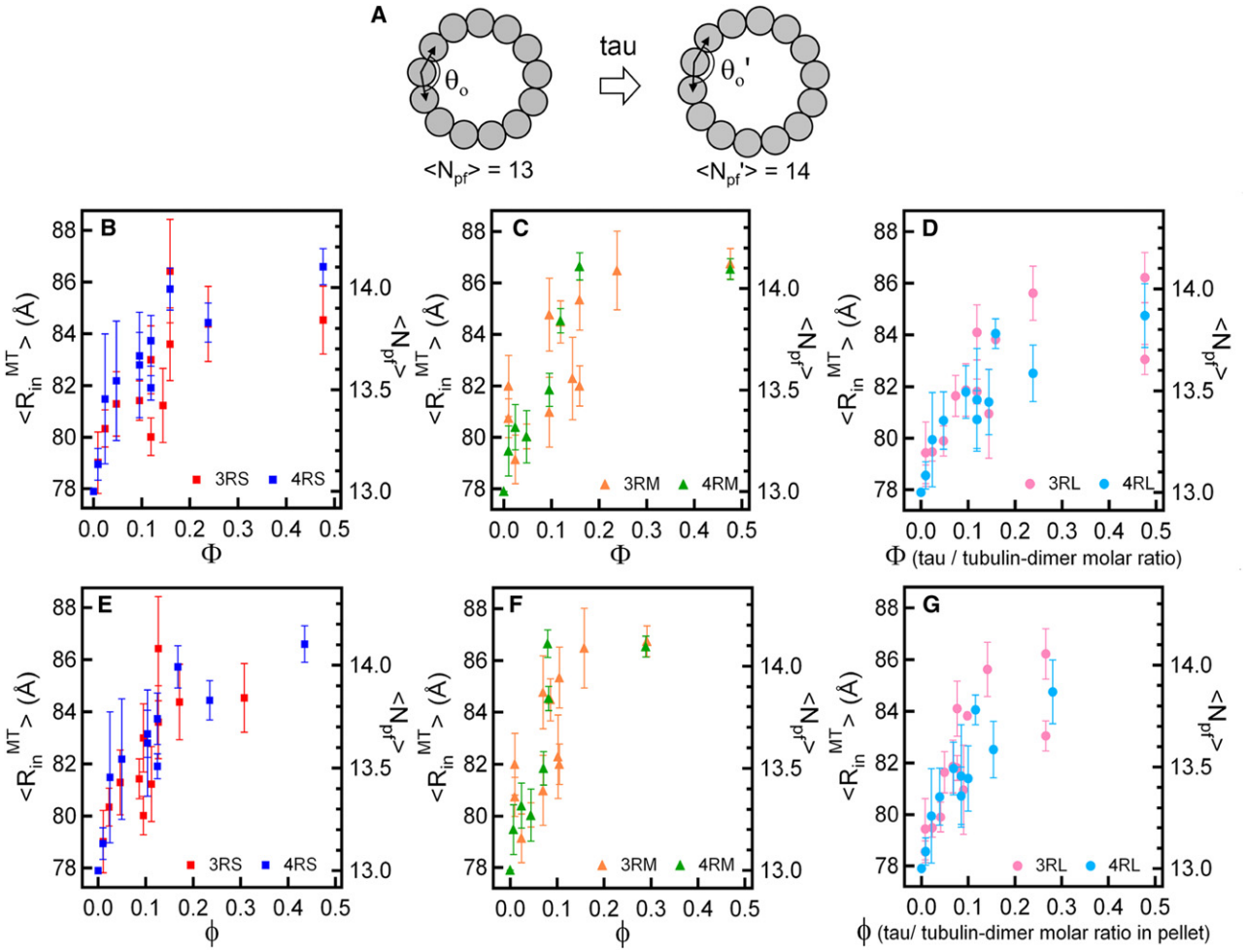

FIGURE 5 (*A*) Schematic showing cross-sections of two MTs showing that with increasing tau binding the distribution of protofilaments in MTs shifts toward MTs with larger N_{pf}, which leads to increases in $\langle R_{in}^{MT}\rangle$. (*B–G*) The inner radius $\langle R_{in}^{MT}\rangle$ for six tau isoforms plotted versus Φ, the tau/tubulin-dimer molar ratio in the reaction mixture (*B–D*), and ϕ, the tau/tubulin-dimer in pellets, which measures only the fraction of tau bound to the MT surface (*E–G*). For all six tau isoforms, the radial size of MTs increases as a function of increasing tau.

The ability for protofilaments to exchange between solvent and MTs or between MTs implies that the energy barrier to breaking and reforming bonds between tubulin-dimers in neighboring protofilaments is of the order of thermal energies.

It is important to highlight the observation from Fig. 5, *E–G*, that the main change in $\langle R_{in}^{MT}\rangle$ occurs at low tau coverage; for example, by $\phi = 0.1$ (1 tau per 10 tubulin-dimers) ≈75% of the change in $\langle R_{in}^{MT}\rangle$ has occurred and the radius saturates for $\phi > 0.15$ (although Fig. 2 *C* shows that tau coverage continues to increase with increasing tau/tubulin-dimer molar ratio in the reaction mixture (Φ)). Thus, a distortion in tubulin dimers on the local scale, due to tau binding, is spread over many MT lattice sites and results in a global change in the distribution of MTs with different numbers of protofilaments. This is a particularly clear demonstration of tau induced change in microtubule structure, which has been suggested previously based on less direct analyses (27,31,41).

To obtain a physical understanding of the mechanism of changes in $\langle N_{pf}\rangle$ one may consider, within the context of a continuum elastic description, the bending elastic energy density $E^{MT} = 0.5\kappa\,(C^{MT} - C_o^{MT})^2$ of a MT due to changes in the protofilament number (33). Here, C_o^{MT} is the spontaneous curvature of a MT, C^{MT} (=$1/R^{MT}$) the curvature of a MT (measured by SAXS) and κ the bending stiffness per unit length associated with the deviations in $\langle N_{pf}\rangle$ from an optimal protofilament number (that determines C_o^{MT}, or equivalently, the optimal spontaneous radius $R_o^{MT} = 1/C_o^{MT}$). In previous work κ has been estimated to be of order 10 k_BT/nm (33).

Fig. 5 *A* depicts a schematic cross-section of two MTs with either 13 or 14 protofilaments, where the angle joining the center of a protofilament to its neighbors is shown to increase to accommodate the added protofilament. This shift in angle is due to changes in the shape of a protofilament, as tau binds, giving rise to a smaller curvature for the MT. Thus, because tau changes the shape of the protofilament it actually

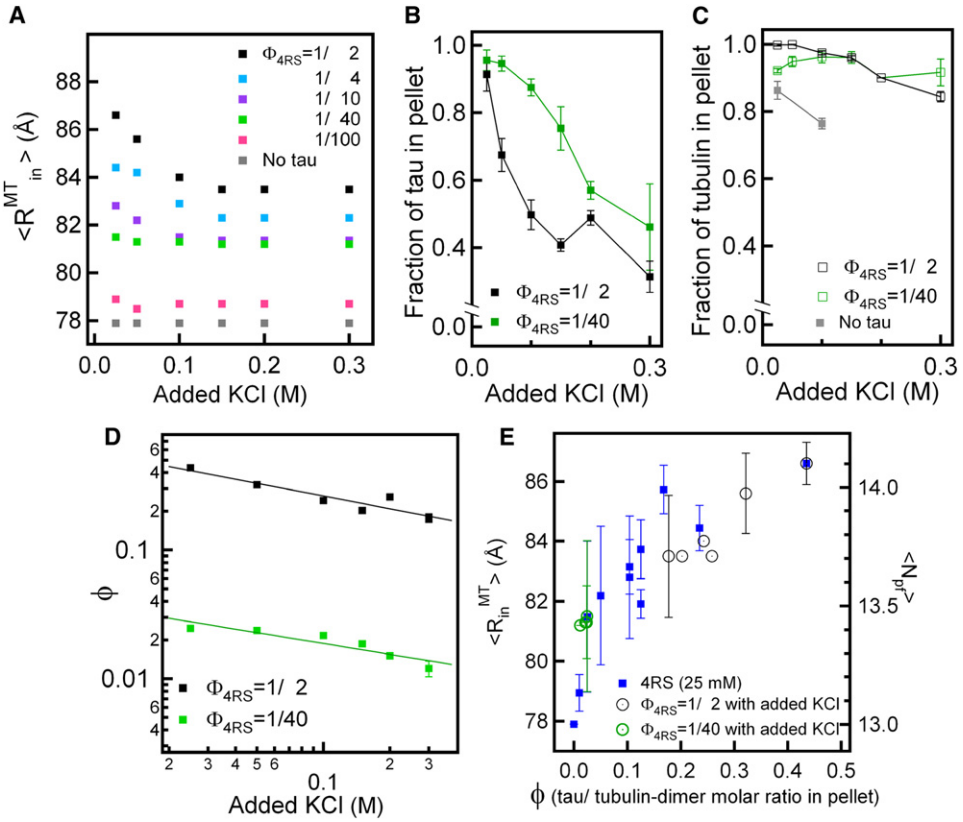

FIGURE 6 Salt dependence of the interactions between tau and MTs. (*A*) The salt dependence of $\langle R_{in}^{MT}\rangle$ for 4RS tau obtained from SAXS data. (*B–D*) Assays measuring the fraction of tau and tubulin in pellets (*B* and *C*) and the decrease in ϕ (tau/tubulin-dimer in pellets) with increasing KCl showing the nonspecific electrostatic nature of tau interactions with MTs (*D*). (*E*) Plot of $\langle R_{in}^{MT}\rangle$ for 4RS tau versus ϕ, where changes in ϕ ($\propto$tau coverage) result from preparations at fixed $\Phi = 1/2$ (*open black circles*) and $\Phi = 1/40$ (*open green circles*) with different amounts of added salt. The blue squares are $\langle R_{in}^{MT}\rangle$ for 4RS tau, in the absence of salt, plotted versus ϕ due to changes in Φ (data from Fig. 5 *E*). For clarity only two typical error bars are plotted for data with open black and green circles.

changes the spontaneous curvature of the MT. A decrease in C_o^{MT} on addition of tau, will lead to a change in the curvature C^{MT}, which tends to approach the value of C_o^{MT} to lower the elastic energy. Because the exact atomic level nature of the tau-MT interaction remains unknown (3,7–9,41–43) we cannot argue why tau decreases rather than increases C_o^{MT}. Rather, we can only assert that the ratio of the projected outer to inner area of a protofilament decreases as tau attaches to the outer surface giving a smaller spontaneous curvature.

We should point out that although tubulin assembly into MTs is an inherently nonequilibrium process (involving GTP hydrolysis), nevertheless, in this study tau is added after the MTs have been stabilized by taxol (with all β-tubulin subunits containing GDP) and one should expect that the system reaches an equilibrium state quite rapidly (33). Changes in the structure of taxol-stabilized MTs, such as exchange of protofilaments between MTs or between solvent and MTs, occur in the absence of energy dissipation (i.e., where no GTP hydrolysis is involved) and should therefore be a direct consequence of the interprotofilament interactions (which, in turn, determine the shape of protofilaments and C_o^{MT}).

Regulation of microtubule radius by tau is salt-dependent

To elucidate the role of nonspecific electrostatic interactions in mediating the binding of tau (through the cationic repeat region) to the MT surface, we used SAXS to measure $\langle R_{in}^{MT}\rangle$ as a function of increasing salt in samples with 4RS tau bound to MTs for $\Phi = 0$, 1/100, 1/40, 1/10, 1/4, and 1/2 (Fig. 6 *A*). In the absence of tau (Fig. 6, *gray squares*) $\langle R_{in}^{MT}\rangle$ is independent of KCl concentration. The largest change in $\langle R_{in}^{MT}\rangle$ is observed for $\Phi = 1/2$ (Fig. 6, *black squares*) where the addition of 0.3 M of KCl leads to a decrease in $\langle R_{in}^{MT}\rangle$ of 3 Å. We see that the final value of $\langle R_{in}^{MT}\rangle \approx 83.8$ Å at high salts is significantly larger than $\langle R_{in}^{MT}\rangle = 77.9$ Å, the inner radius of MTs in the absence of tau. This suggests that some fraction of 4RS tau remains bound to MTs even at 0.3 M of KCl. This is consistent with binding assay measurements as a function of increasing KCl (Fig. 6, *B–D*), which show that for $\Phi = 1/2$, the actual amount of tau bound to MTs (measured by ϕ, the tau/tubulin-dimer in pellet) decreases by $\approx$ a factor of 2 (ϕ decreases from $\approx$0.4 to $\approx$0.19) in going from 25 mM to 0.3 M KCl (Fig. 6 *D*).

Fig. 6 *E* shows data that combines Fig. 6 *A* and Fig. 6 *D* to obtain a plot of $\langle R_{in}^{MT}\rangle$ for 4RS tau versus ϕ, where variations in ϕ ($\propto$tau coverage) are due to different amounts of added salt at fixed $\Phi = 1/2$ (Fig. 6, *open black circles*) and $\Phi = 1/40$ (Fig. 6, *open green circles*). The figure also shows data for $\langle R_{in}^{MT}\rangle$ for 4RS tau, in the absence of salt, versus ϕ (Fig. 6, *blue squares*) due to changes in Φ (data from Fig. 5 *E*). The overlap of the data points, within experimental scatter, implies that the observed salt-dependent behavior of $\langle R_{in}^{MT}\rangle$ (or the salt-dependence of C_o^{MT})

is primarily a result of the actual amount of tau bound to the MT surface. Therefore, KCl suppresses the electrostatic interaction between tau and MTs, resulting in the desorption of tau molecules from microtubules, and a decrease in $\langle R_{\mathrm{in}}^{\mathrm{MT}} \rangle$. This suggests that the dominant force leading to the attachment of 4RS tau to MTs is the electrostatic interaction rather than specific induced fit (shape) interactions.

CONCLUSION

In summary, although it is well appreciated that tau enhances tubulin assembly and regulates MT dynamics, we have discovered that tau isoforms regulate the distribution of protofilament numbers in MTs. In particular, SAXS studies showed that all six tau isoforms increase the average radius of preassembled taxol-stabilized MTs, and that within the scatter of the data, do so in an isoform-independent manner. Additionally, SAXS and binding assay studies under varying monovalent salt conditions showed that the binding forces between 4RS tau and the MT surface are due mostly to nonspecific electrostatic interactions. For all six human wild-type isoforms SAXS showed no evidence of tau-induced MT bundling for tau/tubulin-dimer molar ratios $\Phi \leq 1/2$, which includes the physiologically relevant regime of tau coverage on MT surfaces.

Interestingly, tau isoforms shift the peak in the distribution function describing the MT protofilament number from a mean of 13–14 at tau coverages much less than a monolayer (near physiological conditions) with the tau/tubulin-dimer molar ratio on the order of 0.1. Thus, a local shape distortion in a protofilament due to tau binding is distributed globally over large distances leading to changes in the spontaneous curvature of MTs and the observed shift in the distribution of MT protofilament number. These structural data suggest an allosteric role for MAP tau in axons where the MT surface shape changes, after attachment by tau, may effect the binding affinity of other MAPs to MTs. This is consistent with previous suggestions that tau induces a wave of allosteric changes in microtubule structure, based on the observation that tau can regulate microtubule dynamics when present on MTs at levels of only one tau per several hundred tubulin dimers (27,44). Such an induced allosteric change in tubulin structure could be a mechanistic component of tau's ability to regulate MT dynamics as well as affect the efficacy and regulation of axonal transport, both of which are central to normal and pathological tau action. Additionally, the regulation of the inner MT radius impacts both the mechanical rigidity of MTs and also the availability of the MT lumen (and the inner surface sites) to cellular macromolecules with comparable sizes. Finally, our results should provide insights for controlling the radial size of biological nanotubes for bioengineering applications.

SUPPORTING MATERIAL

A figure is available at http://www.biophysj.org/biophysj/supplemental/S0006-3495(09)00953-9.

We thank R. Beck, R. Bruinsma, Y. Jho, Y.W. Kim, M. Niebuhr, P. Pincus, H. Tsuruta, and T. Weiss for discussions. C.R.S. acknowledges useful discussions with KAIST Faculty where he has a Visiting Professor of Physics appointment. The Stanford Synchrotron Radiation Laboratory, where the x-ray scattering work was carried out, is supported by the United States Department of Energy.

This work was supported by the United States Department of Energy, Division of Material Sciences and Engineering (grant DOE DE-FG02-06ER46314 to C.R.S., M.C.C., U.R., D.J.N.), the United States National Science Foundation (grant NSF DMR-0803103 to C.R.S., M.C.C., U.R., D.J.N.), the National Institutes of Health (grants NS35010 to S.C.F., M.R.G., E.K., D.V., and NS13560 to L.W., H.P.M.), Korea Health 21 R&D Project MOHW (M.W.K.), the Korean Foundation (grant KRF-2005-2214-C00202 to M.C.C.), the International Human Frontier Science Program Organization (U.R.), and the International Human Frontier Science Program Organization Career Development Award (U.R.).

REFERENCES

1. Desai, A., and T. J. Mitchinson. 1997. Microtubule polymerization dynamics. *Annu. Rev. Cell Dev. Biol.* 13:83–117.
2. Chretien, D., F. Metoz, F. Verde, E. Karsenti, and R. H. Wade. 1992. Lattice defects in microtubules: protofilament numbers vary within individual microtubules. *J. Cell Biol.* 117:1031–1040.
3. Andreu, J. M., J. Bordas, J. F. Diaz, J. Garcia de Ancos, R. Gil, et al. 1992. Low resolution structure of microtubules in solution: synchrotron x-ray scattering and electron microscopy of Taxol-induced microtubule assembled from purified tubulin in comparison with glycerol and MAP-induced microtubules. *J. Mol. Biol.* 226:169–184.
4. Andreu, J. M., J. F. Diaz, R. Gil, J. M. de Preda, M. G. de Lacoba, et al. 1994. Solution structure of Taxotere-induced microtubules to 3-nm resolution. *J. Biol. Chem.* 269:31785–31792.
5. Pierson, G. B., P. R. Burton, and R. H. Himes. 1978. Alterations in number of protofilaments in microtubules assembled in vitro. *J. Cell Biol.* 76:223–228.
6. Amos, L. A., and D. Schlieper. 2005. Microtubules and maps. *Adv. Protein Chem.* 71:257–298.
7. Drubin, D. G., and M. W. Kirschner. 1986. Tau protein function in living cells. *J. Cell Biol.* 103:2739–2746.
8. Drubin, D. G., S. C. Feinstein, E. M. Shooter, and M. W. Kirschner. 1985. Nerve growth factor-induced neurite outgrowth in PC12 cells involves the coordinate induction of microtubule assembly and assembly-promoting factors. *J. Cell Biol.* 101:1799–1807.
9. Esmaeli-Azad, B., J. H. McCarty, and S. C. Feinstein. 1994. Sense and antisense transfection analysis of tau function: tau influences net microtubule assembly, neurite outgrowth and neuritic stability. *J. Cell Sci.* 107:869–879.
10. Witman, G. B., D. W. Leveland, M. D. Weingarten, and M. W. Kirschner. 1976. Tubulin requires tau for growth onto microtubule initiating sites. *Proc. Natl. Acad. Sci. USA.* 73:4070–4074.
11. Weingarten, M. D., A. H. Lockwood, S. Y. Hwo, and M. W. Kirschner. 1975. A protein factor essential for microtubule assembly. *Proc. Natl. Acad. Sci. USA.* 72:1858–1862.
12. Caceres, A., and K. S. Kosik. 1990. Inhibition of neurite polarity by tau antisense oligonucleotides in primary cerebellar neurons. *Nature.* 343:461–463.
13. Dawson, H. N., A. Ferreira, M. V. Eyster, N. Ghoshal, L. I. Binder, et al. 2001. Inhibition of neuronal maturation in primary hippocampal neurons from tau deficient mice. *J. Cell Sci.* 114:1179–1187.

14. Kosik, K. S., C. L. Joachim, and D. J. Selkoe. 1986. Microtubule-associated protein tau (tau) is a major antigenic component of paired helical filaments in Alzheimer disease. *Proc. Natl. Acad. Sci. USA*. 83:4044–4048.

15. Selkoe, D. 1991. The molecular pathology of Alzheimer's disease. *Neuron*. 6:487–498.

16. Hutton, M., C. L. Lendon, P. Rizzu, M. Baker, S. Froelich, et al. 1998. Association of missense and 5,-splice-site mutations in tau with the inherited dementia FTDP-17. *Nature*. 393:702–705.

17. Clark, L. N., P. Poorka, Z. Wszolek, D. H. Geschwind, Z. S. Nasreddine, et al. 1998. Pathogenic implications of mutations in the tau gene in pallido-ponto-nigral degeneration and related neurodegenerative disorders linked to chromosome-17. *Proc. Natl. Acad. Sci. USA*. 95:13103–13107.

18. Spillantini, M. G., J. R. Murrell, M. Goedert, M. R. Farlow, A. Klug, et al. 1998. Mutation in the tau gene in familial multiple system tauopathy with presenile dementia. *Proc. Natl. Acad. Sci. USA*. 95:7737–7741.

19. Himmler, A., D. Drechsel, M. W. Kirschner, and D. W. Martin, Jr. 1989. Tau consists of a set of proteins with repeated C-terminal microtubule-binding domains and N-terminal domains. *Mol. Cell. Biol.* 9:1381–1388.

20. Schweers, O., E. Schonbrunn-Hanebeck, A. Marx, and E. Mandelkow. 1994. Structural studies of tau protein and Alzheimer paired helical filaments show no evidence for beta-structure. *J. Biol. Chem.* 269: 24290–24297.

21. Lee, G., N. Cowan, and M. W. Kirschner. 1988. The primary structure and heterogeneity of tau protein from mouse brain. *Science*. 239:285–288.

22. Butner, K. A., and M. W. Kirschner. 1991. Tau protein binds to microtubules through a flexible array of distributed weak sites. *J. Cell Biol.* 115:717–730.

23. Lee, G., R. L. Neve, and K. S. Kosik. 1989. The microtubule binding domain of tau protein. *Neuron*. 2:1615–1624.

24. Goode, B. L., and S. C. Feinstein. 1994. Identification of a novel microtubule binding and assembly domain in the developmentally regulated inter-repeat region of tau. *J. Cell Biol.* 124:769–782.

25. Kosik, K. S., L. D. Orecchio, S. Bakalis, and R. L. Neve. 1989. Developmentally regulated expression of specific tau sequences. *Neuron*. 2:1389–1397.

26. Bunker, J. M., L. Wilson, M. A. Jordan, and S. C. Feinstein. 2004. Modulation of microtubule dynamics by tau in living cells: implications for development and neurodegeneration. *Mol. Biol. Cell*. 15:2720–2728.

27. Panda, D., J. C. Samuel, M. Massie, S. C. Feinstein, and L. Wilson. 2003. Differential regulation of microtubule dynamics by three- and four-repeat tau: implications for the onset of neurodegenerative disease. *Proc. Natl. Acad. Sci. USA*. 100:9548–9553.

28. Toso, R. J., M. A. Jordan, K. W. Farrell, B. Matsumoto, and L. Wilson. 1993. Kinetic stabilization of microtubule dynamic instability in vitro by vinblastine. *Biochemistry*. 32:1285–1293.

29. Binder, L. I., A. Frankfurter, and L. I. Rebhun. 1985. The distribution of tau in mammalian central nervous system. *J. Cell Biol.* 101:1371–1378.

30. Levy, S. F., C. A. C. LeBoeuf, M. R. Massie, M. A. Jordan, L. Wilson, et al. 2005. Three- and four-repeat tau regulate the dynamic instability of two distinct microtubule subpopulations in qualitatively different manners. *J. Biol. Chem.* 280:13520–13528.

31. Goode, B. L., M. Chau, P. E. Denis, and S. C. Feinstein. 2000. Structural and functional differences between 3-repeat and 4-repeat tau isoforms. *J. Biol. Chem.* 275:38182–38189.

32. Needleman, D. J., M. A. Ojeda-Lopez, U. Raviv, K. Ewert, J. B. Jones, et al. 2004. synchrotron x-ray diffraction study of microtubules buckling and bundling under osmotic stress: a probe of interprotofilament interactions. *Phys. Rev. Lett.* 93:1981041–1981044.

33. Raviv, U., T. Nguyen, R. Ghafouri, D. J. Needleman, Y. Li, et al. 2007. Microtubule protofilament number is modulated in a stepwise fashion by the charge density of an enveloping layer. *Biophys. J.* 92:278–287.

34. Raviv, U., D. J. Needleman, Y. Li, H. P. Miller, L. Wilson, et al. 2005. Cationic liposome-microtubule complexes: pathways to the formation of two-state lipid-protein nanotubes with open or close ends. *Proc. Natl. Acad. Sci. USA*. 102:11167–11172.

35. Lee, J., R. P. Frigon, and S. Timasheff. 1973. The chemical characterization of calf brain microtubule protein subunits. *J. Biol. Chem.* 248:7253–7262.

36. Amos, L. A. 1995. The microtubule lattice- 20 years on. *Trends Cell Biol.* 5:48–51.

37. Li, H., D. J. DeRosier, W. V. Nicholson, E. Nogales, and K. H. Downing. 2002. Microtubule structure at 8 Å resolution. *Structure*. 10:1317–1328.

38. Kohn, J. E., I. S. Millett, J. Jacob, B. Zagrovic, T. M. Dillon, et al. 2004. Random-coil behavior and the dimensions of chemically unfolded proteins. *Proc. Natl. Acad. Sci. USA*. 101:12491–12496, (Erratum in Proc. Natl. Acad. Sci. USA. 2005. 102:14475).

39. Elie-Caille, C., F. Severin, J. Helenius, J. D. Howard, and D. J. Muller. 2007. Straight GDP-tubulin protofilaments form in the presence of Taxol. *Curr. Biol.* 17:1765–1770.

40. Zhu, J., J. Hartman, R. Case, S. Rice, and R. Vale. 2007. In-vitro studies of microtubule structures using the MAC mode TM AFM. Molecular Imaging Corporation Application Notes.http://cp.literature.agilent.com/litweb/pdf/5989–6625EN.pdf.

41. Makrides, V., T. E. Shen, R. Bhatia, B. L. Smith, J. Thimm, R. Lal, et al. 2003. Microtubule-dependent oligomerization of tau. Implications for physiological tau function and tauopathies. *J. Biol. Chem.* 278: 33298–33304.

42. Schaap, I. A., B. Hoffmann, C. Carrasco, R. Merkel, and C. F. Schmidt. 2007. Tau protein binding forms a 1 nm thick layer along protofilaments without affecting the radial elasticity of microtubules. *J. Struct. Biol.* 158:282–292.

43. Al-Bassam, J., R. S. Ozer, D. Safer, S. Halpain, and R. A. Milligan. 2002. MAP2 and tau bind longitudinally along the outer ridges of microtubule protofilaments. *J. Cell Biol.* 157:1187–1196.

44. Panda, D., B. L. Goode, S. C. Feinstein, and L. Wilson. 1995. Kinetic stabilization of microtubule dynamics at steady state by tau and microtubule-binding domains of tau. *Biochemistry*. 34:11117–11127.